

## Sijia Zhang

Department of Bioengineering,  
University of Pennsylvania,  
240 Skirkanich Hall,  
210 South 33rd Street,  
Philadelphia, PA 19104  
e-mail: sijiaz@seas.upenn.edu

## Xuan Cao

Department of Materials  
Science and Engineering,  
University of Pennsylvania,  
3231 Walnut Street,  
Philadelphia, PA 19104  
e-mail: xuancao@seas.upenn.edu

## Alec M. Stablow

Department of Bioengineering,  
University of Pennsylvania,  
240 Skirkanich Hall,  
210 South 33rd Street,  
Philadelphia, PA 19104  
e-mail: stablowa@seas.upenn.edu

## Vivek B. Shenoy

Department of Bioengineering,  
University of Pennsylvania,  
3231 Walnut Street,  
Philadelphia, PA 19104;  
Department of Materials  
Science and Engineering,  
University of Pennsylvania,  
3231 Walnut Street,  
Philadelphia, PA 19104;  
Department of Mechanical Engineering and  
Applied Mechanics,  
University of Pennsylvania,  
3231 Walnut Street,  
Philadelphia, PA 19104  
e-mail: vshenoy@seas.upenn.edu

## Beth A. Winkelstein<sup>1</sup>

Mem. ASME  
Department of Bioengineering,  
University of Pennsylvania,  
240 Skirkanich Hall,  
210 South 33rd Street,  
Philadelphia, PA 19104;  
Department of Neurosurgery,  
University of Pennsylvania,  
240 Skirkanich Hall,  
210 South 33rd Street,  
Philadelphia, PA 19104  
e-mail: winkelst@seas.upenn.edu

# Tissue Strain Reorganizes Collagen With a Switchlike Response That Regulates Neuronal Extracellular Signal-Regulated Kinase Phosphorylation In Vitro: Implications for Ligamentous Injury and Mechanotransduction

*Excessive loading of ligaments can activate the neural afferents that innervate the collagenous tissue, leading to a host of pathologies including pain. An integrated experimental and modeling approach was used to define the responses of neurons and the surrounding collagen fibers to the ligamentous matrix loading and to begin to understand how macroscopic deformation is translated to neuronal loading and signaling. A neuron-collagen construct (NCC) developed to mimic innervation of collagenous tissue underwent tension to strains simulating nonpainful (8%) or painful ligament loading (16%). Both neuronal phosphorylation of extracellular signal-regulated kinase (ERK), which is related to neuroplasticity ( $R^2 \geq 0.041$ ;  $p \leq 0.0171$ ) and neuronal aspect ratio (AR) ( $R^2 \geq 0.250$ ;  $p < 0.0001$ ), were significantly correlated with tissue-level strains. As NCC strains increased during a slowly applied loading (1%/s), a “switchlike” fiber realignment response was detected with collagen reorganization occurring only above a transition point of 11.3% strain. A finite-element based discrete fiber network (DFN) model predicted that at bulk strains above the transition point, heterogeneous fiber strains were both tensile and compressive and increased, with strains in some fibers along the loading direction exceeding the applied bulk strain. The transition point identified for changes in collagen fiber realignment was consistent with the measured strain threshold (11.7% with a 95% confidence interval of 10.2–13.4%) for elevating ERK phosphorylation after loading. As with collagen fiber realignment, the greatest degree of neuronal reorientation toward the loading direction was observed at the NCC distraction corresponding to painful loading. Because activation of neuronal ERK occurred only at strains that produced evident collagen fiber realignment, findings suggest that tissue strain-induced changes in the micromechanical environment, especially altered local collagen fiber kinematics, may be associated with mechanotransduction signaling in neurons.*

[DOI: 10.1115/1.4031975]

*Keywords:* ligament, pain, mechanotransduction, collagen, biomechanics, discrete fiber network model

## Introduction

Although ligaments function to primarily stabilize joints, they are increasingly recognized as sensory organs due to their afferent innervation, providing both mechanoreceptive and nociceptive feedback [1–4]. The mechanical and neurological functions of

ligaments can produce a variety of musculoskeletal pathologies [5]. For example, neck pain, a common musculoskeletal disorder, can originate from spinal ligaments [6]. In particular, the facet capsular ligament (FCL) that encloses the spinal facet joints is a common source of pain due to neck trauma [7–9]. Biomechanical and neurophysiological studies in animal models have shown that excessive FCL loading that produces nonphysiologic strains also induces damage to the collagen network and axons of innervating neurons, persistent afferent firing, spinal neuronal hypersensitivity, and altered neurotransmitter expression, as well as pain

<sup>1</sup>Corresponding author.

Manuscript received August 5, 2015; final manuscript received October 21, 2015; published online January 27, 2016. Editor: Victor H. Barocas.

[7,10–18]. Although injurious ligament loading is known to activate nociceptors for pain signaling, the local biomechanical mechanisms by which neurons are injured, their biomechanical vulnerability, and the resulting physiological dysfunction are still poorly understood.

Cells respond to changes in the mechanical microenvironment via adhesive interactions with the extracellular matrix (ECM) [19,20]. Since neurons embedded in a collagen matrix have passive mechanical roles due to their lack of contractility and high compliance compared to the surrounding matrix [21–23], they can be loaded and oriented via collagen fiber deformation and realignment during tissue loading. Unlike direct mechanical insults to nerves, excessive ligament stretch presents a more complex injury modality involving both functional impairment of neurons and disruption of the ECM. Studies using advanced imaging techniques and computational modeling have reported that collagen fibers realign and generate fiber forces to accommodate macroscopic deformation in ligaments and artificial collagen networks [24–26]. We have shown previously that subfailure FCL loading exceeding physiologic strains produces microstructural injury and collagen disorganization in human FCLs [16,27,28], which presents a mechanism by which external tissue loading may be transmitted to neurons and induce mechanotransduction. Since the ligament can undergo varied strain magnitudes and strain rates during injury [29,30] and since strain rate modulates ligament tension [5,31], collagen reorganization in cyclic loading [32], and cell viability and permeability [33,34], both strain magnitude and rate are hypothesized to regulate the micromechanical environment of the neurons embedded in the ligament and, thereby, modulate their responses during tissue loading. However, no study has defined the relationships between tissue-level mechanics, collagen micromechanics, and neuronal responses under different loading conditions for ligament systems with embedded neurons.

Many types of neurons respond differently to varied mechanical stimuli and are sensitive to touch, proprioception, and/or pain [35]. Deformation of neuronal membranes activates mechanosensitive ion channels and cell surface receptors, which transform any applied mechanical stress into electrical signals and modulate expression of a host of molecules involved in a wide range of cellular functions [35–38]. Activation of the ERK pathway by phosphorylation can be induced by cellular deformation [39–41]. Further, fast phosphorylation of ERK after mechanical stimuli has been hypothesized to mediate neuronal plasticity and to increase neuronal excitability by modulating the gating properties of specific sodium channels [42–44]. As such, expression of phosphorylated ERK (pERK) has been used as an indicator of neuronal activation in both the peripheral and central nervous systems [43–46]. Investigating neuronal deformation and activation due to external tissue loading is often confounded by complex mechanics of fibers in the ECM. To understand how fiber motion and deformation regulate neuronal responses under tissue loading, changes in the local collagen network and neuronal activity, such as ERK phosphorylation, need to be measured simultaneously.

Ligament injury is commonly studied using *ex vivo* tissue testing and animal models. Although mechanical testing of isolated ligaments enables evaluation of tissue mechanics across different length scales, measurement of physiological cellular responses is challenging. In addition, it is difficult to measure collagen fiber and network biomechanics during ligament loading *in vivo*. Although we and others have integrated quantitative polarized light imaging (QPLI) techniques with mechanical testing to define collagen fiber kinematics in real time during tensile loading of isolated ligaments and cell-compacted collagen-based gels [24,25,47,48], those approaches are unable to measure microscopic fiber stresses and strains. Computational models, such as finite-element based two-dimensional (2D) DFN models, have been developed to systematically examine the large parameter space of properties of a fibrous matrix with cells embedded in it and to predict collagen fiber stretch at different bulk tissue strains [26,49–52]. In particular, the DFN model has been used to predict heterogeneous fiber deformations and realignment due to cell

contraction that leads to force transmission in randomly organized networks [49], providing a platform to estimate microscopic fiber mechanics. In order to measure both local collagen mechanics and neuronal responses and to evaluate their relationships, combined experimental and modeling approach is needed.

The aim of this study was to define how macroscopic tissue deformations modulate neuronal responses via regulation of microstructural collagen mechanics, using complementary experimental and computational methods. In the first study, we developed a three-dimensional (3D) *in vitro* NCC system that mimics the innervation of ligaments in order to enable the measurement of macro- and microscale tissue mechanics, matrix reorganization, and neuronal responses. Separate groups of NCCs were distracted to displacement magnitudes simulating FCL strains that are associated with either nonpainful (8% strain) or painful (16% strain) states *in vivo* [10,28,53] at rates of 0.5 mm/s (1%/s) and 3.5 mm/s (7%/s), which simulate physiologic loading conditions across sevenfold difference in strain rate [54,55]. Expression of pERK in neurons, neuron shape and orientation, and collagen fiber realignment after NCC loading was each evaluated to test the effects of strain magnitude and loading rate on the neuronal responses and collagen reorganization. Logistic regression was used to determine if a strain threshold for neuronal activation exists between the physiologic and nonphysiologic mechanical loading regimes and if that transition relates to collagen reorganization. In addition, a DFN model was created using the collagen fiber density, length, and orientation distributions of the NCCs, and that model was validated by comparing the predicted fiber reorientation to that measured experimentally. We then used that DFN model to predict fiber strains in order to begin to understand the local biomechanical mechanisms by which neurons are loaded and respond to nonphysiologic tissue deformations.

## Materials and Methods

**Neuronal Culture and NCC System.** All animal procedures were approved by the Institutional Animal Care and Use Committee at the University of Pennsylvania. Cortical neurons were isolated from embryonic day 18 Sprague-Dawley rats as described previously [56]. Briefly, timed pregnant rats were anesthetized with 5% CO<sub>2</sub> and terminated by cervical dislocation. Embryos were surgically removed and the neocortical tissue was dissected, dissociated in trypsin (1.4 mg/ml; Life Technologies, Frederick, MD) and DNase (0.6 mg/ml; Roche Applied Science, Indianapolis, IN) for 15 min at 37 °C and underwent trituration and filtration through Nitex mesh (Crosswire Cloth Bellmawr, NJ). Isolated cells were resuspended in plating medium containing Minimum Essential Media with Earle's salts (Life Technologies, Frederick, MD) and GlutaMAX (Life Technologies, Frederick, MD) supplemented with 0.6% D-glucose (Sigma-Aldrich, St. Louis, MO), 1% Pen-Strep (Life Technologies, Frederick, MD), and 10% horse serum (Life Technologies, Frederick, MD), and plated on poly-D-lysine (0.08 mg/ml; Sigma-Aldrich, St. Louis, MO) and laminin-coated (0.001 mg/ml; BD Biosciences, San Jose, CA) T75 flasks.

A collagen solution was prepared using rat tail collagen I (2 mg/ml; Corning Inc., Corning, NY) and cast in a dog-bone shaped Teflon mold for gelation at 37 °C overnight [48]. The dog-bone shaped construct is 62.5 mm long, 23.5 mm wide, and 3 mm thick with the middle narrow section being 31.5 mm long and 7.5 mm wide. Neurons were then replated onto the prepared collagen gels at a density of 10<sup>7</sup> cells/ml (~4500 cells/mm<sup>2</sup>) and were allowed to grow in the feeding medium containing Neurobasal Media (Life Technologies, Frederick, MD) supplemented with 2% B-27 (Life Technologies, Frederick, MD), 0.2% GlutaMAX, and 1% Pen-Strep for 2 days *in vitro* (DIV) in a humidified 37 °C 5% CO<sub>2</sub> incubator. Additional collagen solution was added on DIV 4 to encapsulate the neurons in the NCC construct.

**Mechanical Testing and Data Acquisition.** On DIV 8, NCCs were distracted at 0.5 mm/s or 3.5 mm/s to displacements

simulating nonpainful (4 mm;  $n=8$  for 0.5 mm/s,  $n=7$  for 3.5 mm/s) and painful (8 mm;  $n=9$  each of 0.5 mm/s or 3.5 mm/s) FCL loading in vivo [10,28,53]; unloaded constructs ( $n=5$ ) were also included as controls for neuronal shape and ERK phosphorylation in the unloaded resting configuration. NCCs were immersed in a phosphate-buffered saline (PBS)-filled chamber and loaded by an Instron 5865 (Instron, Norwood, MA) that is integrated with a QPLI system (Figs. 1(a) and 1(b)). Fiber alignment maps were acquired from the NCCs before, during, and after loading using the QPLI system as described previously [16,25]. The QPLI system is made up of a fiber-optic illuminator (Dolan-Jenner Industries Inc., Boxborough, MA), a linear polarizer (Edmund Optics, Barrington, NJ) that rotates at 750 rpm, and a customized circular analyzer attached to a high-speed camera (Phantom-v9.1; Vision Research Inc, Wayne, NJ) (Fig. 1(a)). The birefringent NCC sample was placed between the rotating polarizer and the circular analyzer (Fig. 1(a)). Images were collected at 500 fps with a resolution of 14.5 pixel/mm and pixelwise fiber alignment maps were created in MATLAB (R2014a, MathWorks Inc., Natick, MA) based on a harmonic equation using every 20 consecutive images [24,27]. Circular variance, a measure of the spread of dihedral angles with a lower value representing tighter clustering [57,58], was used to quantify the fiber alignment before, during and after loading for each NCC. The circular variances measured at the maximum displacement for each loading condition and each NCC were normalized to the unloaded reference level, which was measured before application of load, in order to assess the degree of fiber realignment.

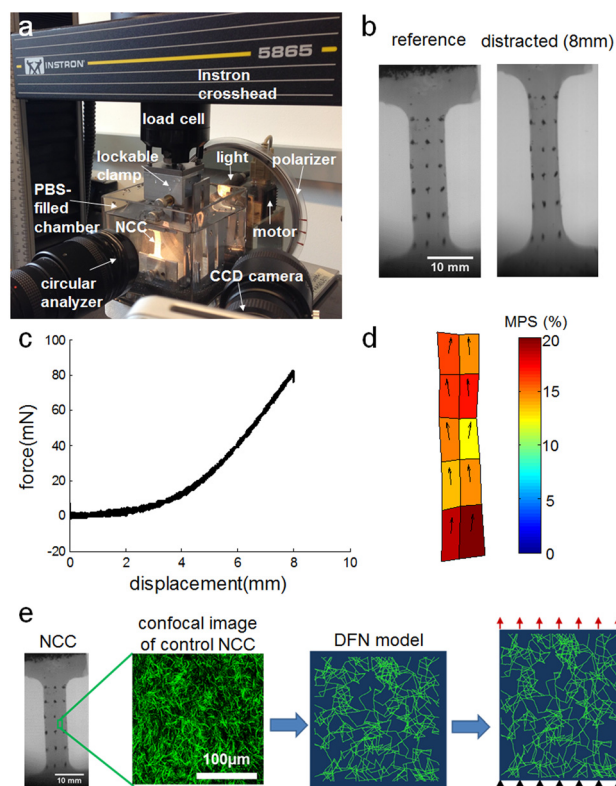


**Fig. 1** Representative images of the experimental test setup demonstrating (a) the mechanical testing system integrated with the elements of the QPLI system, (b) an NCC in an unloaded reference state and at 8 mm of distraction, (c) the corresponding force–displacement response, and (d) strain map showing both the magnitude and directions of MPS at 8 mm displacement. (e) A schematic overview showing the DFN model as constructed using the confocal images of collagen in elements of the unloaded control NCCs, as well as the boundary conditions simulating experimental conditions for the NCCs.

The force and displacement data collected during loading (Fig. 1(c)) were used to ensure that no failure occurred and to determine the maximum stiffness and the maximum force during NCC loading. Stiffness was calculated by differentiating the force–displacement data using a centered finite-difference approximation as described previously [27], at 0.5 mm displacement increments throughout loading. In addition, each NCC had a grid of fiducial markers on it, which were used to track regional deformations and to estimate strains in ten four-node elements on each gel surface (Figs. 1(b) and 1(d)). Marker displacements were recorded during loading and processed in MATLAB to construct a finite-element mesh in LS-DYNA (Livermore Software Technology Corp., Livermore, CA), which was used to estimate maximum principal strain (MPS) maps (Fig. 1(d)) [59,60]. Bulk strain was defined as the overall MPS across the entire gel and was measured by tracking the four markers in the corners of the marker grid and using them to create a single four-node element for each NCC. The MPS estimated in each of the ten four-node elements of each gel was also calculated as the elemental strain; elemental strains were used to relate local/regional strains to neuronal responses. At the limit of the applied distraction (either 4 mm or 8 mm depending on the group), the NCCs were held fixed using customized lockable clamps (Fig. 1(a)); together, the clamps and sample were removed from the mechanical test frame and fixed for immunocytochemistry processing, in order to measure neuron deformation and orientation. All NCCs were fixed using 4% paraformaldehyde (Sigma-Aldrich, St. Louis, MO) for 2 hrs at room temperature and stored in 30% sucrose (Sigma-Aldrich, St. Louis, MO) in PBS at 4 °C.

**Immunocytochemistry and Analysis of Neuronal pERK Expression, Shape, and Orientation.** Fixed NCCs were blocked using 10% normal goat serum (Vector Laboratories, Burlingame, CA) with 0.3% Triton-X100 (Bio-Rad Laboratories, Hercules, CA) in PBS for 2 hrs and treated with rabbit anti-pERK antibody (1:200; Cell Signaling Technology, Danvers, MA) and chicken anti- $\beta$ III-tubulin antibody (1:200; Abcam, Cambridge, MA) for 36 hrs at 4 °C to label pERK and neurons, respectively. NCCs were then washed with PBS and incubated for 2 hrs in the secondary antibodies goat anti-rabbit Alexa Fluor 568 (1:1000; Life Technologies, Frederick, MD) for pERK and goat anti-chicken Alexa Fluor 488 (1:1000; Life Technologies, Frederick, MD) for  $\beta$ III-tubulin. Three images of each element of each NCC (Fig. 1) were taken using the 40 $\times$  objective of a Zeiss LSM510 confocal microscope (1024  $\times$  1024 pixels; Carl Zeiss Inc., Thornwood, NY). Automated densitometry quantified labeling of total pERK in each image by measuring the percent of positively labeled pixels as described previously [61,62]. Expression of pERK was averaged across images from each element of each NCC sample to define the elemental pERK production in that element.

The elemental pERK expression in loaded gels was normalized to that of the matching control NCCs that were similarly immunolabeled in order to account for any differences between processing. The mean normalized pERK expression of each loading group was calculated by averaging the values across all elements from all NCCs within each group. Neuronal structure was also measured using the confocal images. The cellular aspect ratio (AR) and cell orientation were measured by an assessor blinded to groups in 30 representative cells sampled throughout each NCC (3 cell/element) using ImageJ (National Institutes of Health, Bethesda, MD). Cellular AR was defined as the ratio between the cell's long- and short-axes; cell orientation was defined as the angle difference between the long-axis of the neuron and the applied loading direction. To account for differences in the initial cell shape and orientation between NCCs, phase contrast images of neurons were taken prior to mechanical loading to serve as unloaded references and the mean AR from 30 representative cells was computed for each NCC before loading. Normalized AR after loading was defined as the AR measured in the confocal image

divided by the mean AR from the unloaded NCC and was averaged within each element. Orientation angles were only measured in noncircular cells exhibiting identifiable long-axes among the 30 selected cells from each NCC.

**Data and Statistical Analyses.** All statistical tests were performed in JMP (version 11, SAS Institute, Cary, NC), with significance at  $p < 0.05$ . Differences in the maximum force and stiffness, pERK expression, normalized circular variance, and cell orientation angles between different groups were evaluated using separate two-way analysis of variance (ANOVA) with distraction magnitude and rate as the two factors. If significant differences were detected due to the interaction effect of strain magnitude and rate, post-hoc Tukey honestly significant difference tests were performed.

The relationships between elemental MPS and each of normalized pERK expression and normalized AR were tested by correlation analysis using linear regression models for each distraction rate separately. The relationship between elemental MPS and collagen fiber realignment was also examined using a linear regression model. Each of the mean circular variance and the mean MPS was computed separately at the 0.5 mm displacement increments during loading and the circular variance was plotted against the MPS. The correlation between the circular variance and MPS was tested using a two-phase linear regression model, which also estimated the transition point between the two phases [63–65]. The significance of each of the regressions was evaluated using F-tests.

Strain thresholds for increasing ERK phosphorylation were estimated using logistic regressions [66,67]. Normalized pERK expression was binarized based on if the ERK phosphorylation was increased due to loading; if the normalized pERK expression in an element was greater than 1 immediately after loading, ERK phosphorylation in that element was considered to be higher than the unloaded control level. Unloaded controls were included and the pERK expression was taken as 0. Binarized pERK expression was plotted against elemental MPS and fitted using logistic regressions. The 50th- and 95th-percentile MPS with 95% confidence intervals for elevated ERK phosphorylation were determined for, and compared between, groups with different loading rates.

**DFN Modeling and Collagen Fiber Mechanics.** An image-based DFN model was constructed based on the NCC structure to measure collagen micromechanics. To measure the average microstructure of the collagen network in the NCCs, four unloaded control gels were immunolabeled for collagen I using a mouse anticollagen I antibody (1:400; Abcam) and a secondary goat anti-mouse Alexa Fluor 488 antibody (1:1000; Invitrogen); NCCs were imaged using confocal microscopy as described above. The average collagen fiber density and length measured from confocal images of those four control NCCs were used as network parameters to create a comparable fibrous network (Fig. 1(e)) as described previously [49]. Fiber diameter, length, and density were assumed to be 250 nm [49], 28.7  $\mu\text{m}$ , and 9621 fibers/ $\text{mm}^2$ , respectively. The initial fiber orientation distribution was assigned to be uniform, because the NCCs were created with random fiber organization. Collagen fibers were treated as linear elastic materials with rigid crosslinks and modeled using shear flexible Timoshenko beam elements in ABAQUS [49]. Each fiber section between two crosslinks was meshed into four elements based on prior convergence studies with this DFN model [49]. Uniaxial tension was applied to the network model with the same boundary conditions as in the NCC experiment (Fig. 1(e)). The bottom of the network was held fixed and the top boundary edge was distracted along the vertical direction, with the sides allowed to undergo unconstrained movement. Fiber orientation and axial strains were computed throughout the network before loading and at bulk strains of 7% and 16%, which correspond to strain magnitudes that are either nonpainful or painful, respectively, in vivo

[10,28,53]. To quantify the changes in the fiber angle distribution after stretch in the DFN model, the Chi-squared goodness-of-fit approach was used to measure the deviation from the initial uniform fiber angle distribution, with a higher Chi-squared value indicating a less uniform distribution [68].

## Results

Both distraction magnitude and rate altered the maximum force ( $p < 0.006$ ) and maximum stiffness ( $p \leq 0.0004$ ) of the loaded NCCs (Table 1). Not surprisingly, increasing the magnitude of distraction significantly increased both the bulk MPS ( $p < 0.0001$ ) and the mean elemental MPS ( $p < 0.0001$ ) (Table 1). The strains in the NCC were doubled for corresponding doubling of applied distraction, regardless of the loading rates used in this study (Table 1).

The amount of ERK phosphorylation increased with the extent of loading (Table 1; Fig. 2) and was correlated with the local elemental MPS (Fig. 3). The amount of pERK normalized to control levels was significantly elevated ( $p \leq 0.002$ ) in NCCs distracted to 8 mm compared to the levels expressed at 4 mm, for both of the distraction rates (Fig. 2). However, pERK expression was not different between the two loading rates at either distraction magnitude (Fig. 2). Further, normalized pERK expression and elemental MPS were correlated at both rates, with weak, but significant, correlations at both 0.5 mm/s ( $R = 0.447$ ;  $p < 0.0001$ ) and 3.5 mm/s ( $R = 0.202$ ;  $p = 0.0171$ ) (Fig. 3(a)). Of note, although weak, the production of pERK was more strongly correlated with elemental MPS under the slower loading rate (0.5 mm/s) than the faster rate (3.5 mm/s) (Fig. 3(a)).

The strain thresholds for elevated ERK phosphorylation were also similar between the two loading rates, with slightly higher thresholds for slower loading (Fig. 3(b)). Logistic regression of the binarized pERK expression against the elemental MPS predicted a 50th-percentile threshold of 11.7% (95% confidence interval: 10.2–13.4%) for 0.5 mm/s loading and a threshold of 10.2% (95% confidence interval: 8.7–12.0%) for tensile loading applied at 3.5 mm/s (Fig. 3(b)). In addition, the 95th-percentile MPS for increased pERK production was estimated at 24.9% (95% confidence interval: 21.6–30.1%) at 0.5 mm/s and 23.7% (95% confidence interval: 20.3–29.6%) at 3.5 mm/s. The logistic regressions were run separately for each distraction rate and were significant ( $p < 0.0001$ ).

Neuronal AR and orientation due to loading were also affected by the loading parameters, but in different ways. For example, AR increased with increasing elemental MPS, but the cell orientation response during loading was different for the rate of loading (Fig. 4). At the unloaded reference configuration, most neurons were circular and there was no difference detected in cell shape and orientation between any group. After loading, the normalized AR displayed significant positive correlations with elemental MPS at both 0.5 mm/s ( $R = 0.500$ ,  $p < 0.0001$ ) and 3.5 mm/s ( $R = 0.742$ ,  $p < 0.0001$ ) rates (Fig. 4(a)). In addition, the cell orientation distribution responses (Fig. 4(b)) were significantly different ( $p = 0.004$ ) at the slower (0.5 mm/s) and faster (3.5 mm/s) loading rates after NCC distraction. The long-axes of neurons in NCCs loaded at 0.5 mm/s to 8 mm were more aligned with the loading direction than those neurons in NCCs distracted to 8 mm at 3.5 mm/s (Fig. 4(c)). Further, more neurons remained circular with no identifiable long-axis in gels loaded only to 4 mm compared to neurons in gels loaded to 8 mm at the 0.5 mm/s, resulting in a lower probability of aligning neurons toward the loading direction at the nonpainful smaller distraction magnitude (Fig. 4(c)).

More collagen fiber realignment was evident with increased distraction magnitude and was greater for the slower loading rate. In the unloaded reference configuration, the average collagen fiber direction was approximately 0 deg (Fig. 5(a)), which was consistent with the initial random fiber orientation. With increased imposed distraction, the collagen fiber realignment that was observed in all groups was toward the loading direction, as indicated by the orientation vectors in the alignment maps (Fig. 5(a)).

**Table 1 Summary of mechanics, pERK production, and fiber alignment for NCCs**

Displacement (mm)	Rate (mm/s)	Specimen	Maximum		Average			
			Force (mN)	Stiffness (mN/mm)	Bulk MPS (%)	Elemental MPS (%)	Normalized pERK expression	Normalized circular variance
4	0.5	1	21.6	5.7	7.88	8.55	0.75	NA
		2	16.7	6.7	7.74	8.79	0.90	NA
		3	18.6	8.2	8.53	9.60	0.91	NA
		4	27.4	12.7	7.54	7.49	0.96	3.93
		5	7.8	5.8	6.04	6.22	0.72	1.40
		6	3.2	4.2	9.60	9.76	1.14	0.41
		7	6.5	2.9	8.55	8.98	0.75	1.83
		8	13.7	5.8	7.79	7.82	1.03	0.62
		Mean	14.4	6.5	7.96	8.40	0.90	1.64
		SD	7.7	2.8	0.96	1.10	0.14	1.40
4	3.5	1	30.4	18.6	6.15	6.18	1.01	NA
		2	20.6	4.7	5.50	5.90	1.02	NA
		3	26.5	9.6	6.36	7.22	0.96	NA
		4	25.5	8.3	5.46	6.11	0.91	NA
		5	19.6	10.8	9.23	9.12	0.96	1.23
		6	29.4	15.7	8.34	9.31	1.33	1.17
		7	30.4	20.6	8.57	8.47	1.06	1.95
		Mean	26.0	12.6	7.09	7.48	1.04	1.45
		SD	4.2	5.4	1.46	1.37	0.13	0.43
		8	0.5	1	49.0	12.0	13.37	12.44
2	59.8			11.5	15.77	15.75	0.97	NA
3	79.4			21.7	17.86	18.12	1.48	NA
4	100.9			23.9	18.96	19.50	1.44	NA
5	97.0			22.7	15.57	15.47	0.74	98.5
6	112.7			29.6	16.52	16.48	1.35	259.7
7	76.4			32.4	12.92	14.21	1.18	36.5
8	82.3			21.9	18.35	18.95	1.53	56.2
9	78.4			24.3	18.93	19.11	1.96	155.0
Mean	81.8 <sup>a</sup>			22.2 <sup>a</sup>	16.47 <sup>a</sup>	16.67 <sup>a</sup>	1.31 <sup>a</sup>	121.2 <sup>a</sup>
SD	19.9	6.9	2.27	2.44	0.35	89.8		
8	3.5	1	123.5	38.2	15.13	14.48	1.21	NA
		2	95.1	32.3	16.06	15.81	1.14	NA
		3	121.5	27.4	13.86	13.33	1.21	NA
		4	73.5	28.4	12.12	11.94	1.36	NA
		5	168.6	51.0	14.23	14.55	1.21	48.8
		6	79.4	26.5	15.43	16.01	1.09	1.7
		7	135.2	33.3	17.18	16.85	1.04	54.3
		8	104.9	30.4	17.84	17.21	1.12	15.9
		9	96.0	31.4	17.21	17.00	2.84	8.9
		Mean	110.8 <sup>b,c</sup>	33.2 <sup>b,c</sup>	15.45 <sup>b</sup>	15.24 <sup>b</sup>	1.36 <sup>b</sup>	25.9 <sup>c</sup>
SD	29.8	7.5	1.85	1.81	0.56	24.0		

<sup>a</sup>Significant difference compared to the 4 mm, 0.5 mm/s group ( $p \leq 0.009$ ).

<sup>b</sup>Significant difference compared to the 4 mm, 3.5 mm/s group ( $p \leq 0.002$ ).

<sup>c</sup>Significant difference compared to the 8 mm, 0.5 mm/s group ( $p \leq 0.040$ ).

Tensile loading to 8 mm induced nonuniform fiber reorganization across the entire NCC, with the most realignment evident along the free boundaries where the lateral contraction was the greatest (Fig. 5(a)). As with the orientation of neurons toward the loading direction (Fig. 4(c)), the greatest degree of fiber realignment, indicated by a high normalized circular variance, was induced at 8 mm under slower applied tension (0.5 mm/s). The degree of fiber realignment in NCCs distracted to 8 mm at slower rate was significantly greater ( $p \leq 0.040$ ) than the collagen fiber reorganization in any of the other loading conditions (Fig. 5(b)).

The circular variance of fiber orientation exhibited a two-phase response to increasing bulk strain, with little change initially at small strains followed by a rapid increase with increasing strain (Fig. 5(c)). A two-phase linear regression model identified a switchlike transition between isotropic and anisotropic collagen reorganization based on changes in the circular variance. That modeling identified 11.3% strain as the transition point between the two phases of fiber realignment (Fig. 5(c)), a strain value very close to the 50th-percentile strain threshold (11.7%) identified for

elevated pERK production at this rate of applied tension (Fig. 3(b)). At strains below that transition point, the average fiber orientation angle of the isotropic collagen matrix remained near 0 deg ( $0.47 \pm 6.66$  deg), with a small-to-negligible circular variance ( $0.001 \pm 0.001$ ) (Fig. 5(c)). Beginning at a strain of  $11.6 \pm 1.8\%$ , the circular variance began to increase substantially, rising to  $0.122 \pm 0.056$  at  $16.8 \pm 2.2\%$  strain (Fig. 5(c)). This over 100-fold increase in the circular variance induced by NCC loading reflected a mean fiber realignment of  $12.2 \pm 11.0$  deg that was averaged across all the NCCs (Figs. 5(a) and 5(c)). The distribution of fiber orientation angles displayed a tight cluster around 0 deg before loading was applied (at 0% strain) and a high degree of dispersion, with peaks at  $\pm 90$  deg, after distraction to 16% strain (Fig. 5(c)), which indicated a strong realignment in the direction of loading with increased strain.

Fiber realignment predicted by the DFN model was consistent with the experimental observations and also illustrated the switchlike response of fiber network reorganization (Figs. 5(c) and 6). For small strains below the 11.3% transition point, such as 7%,

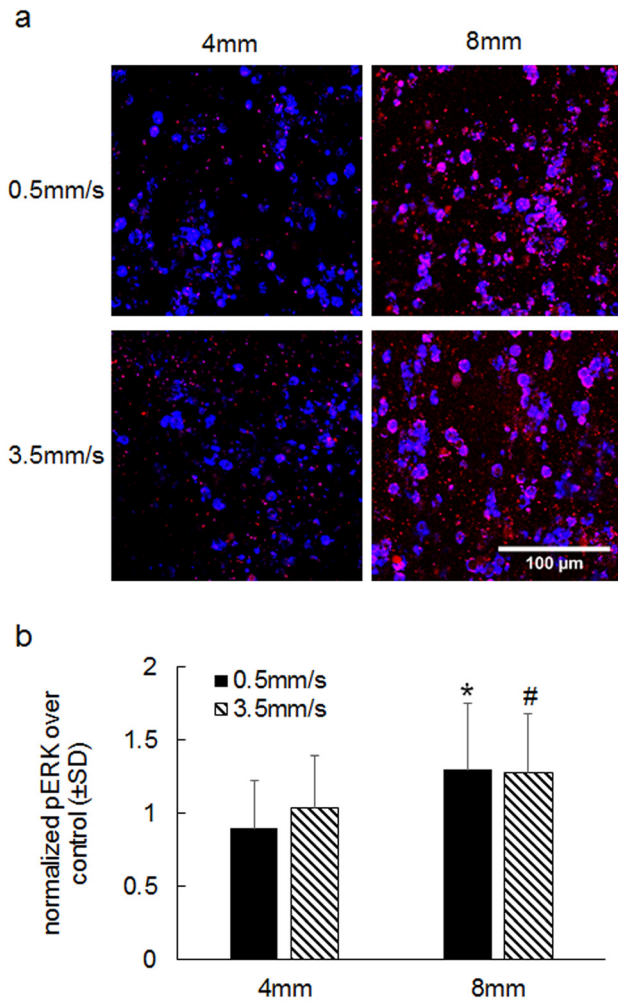


**Fig. 2** ERK phosphorylation increases with increasing imposed distraction magnitude. (a) Representative confocal images showing neuronal structure labeled for  $\beta$ III-tubulin (blue), pERK expression (red), and their colocalization (pink) demonstrate increased ERK phosphorylation at 8 mm than at 4 mm but with no difference for loading rate; the scale bar applies to all panels. (b) Quantification of pERK expression in loaded constructs normalized to unloaded controls indicates significant increases in NCCs distracted to 8 mm compared to 4 mm at both the 0.5 mm/s ( $*p < 0.0001$ ) and 3.5 mm/s ( $\#p = 0.002$ ) distraction rates.

fiber alignment remained similar to the initial distribution that was uniform (Fig. 6(a)). However, at a larger strain of 16%, which was greater than the transition point, there was preferable reorientation of fibers in the model toward the loading direction (Fig. 6(a)). The DFN model also predicted heterogeneous collagen fiber strains, with fibers undergoing both tension and compression (Figs. 6(b) and 6(c)). Most fibers underwent axial strains that were less than the applied bulk strain. For example, at 16% bulk strain, the majority of fibers underwent  $\sim 5\%$  to  $10\%$  strain (Fig. 6(c)). As more collagen fibers realigned toward the loading direction with increasing bulk strain, the distribution of the fiber axial strains exhibited increased fiber counts and higher dispersion at high fiber strains, with a few load-bearing fibers exhibiting axial strains that were actually greater than the applied bulk strain (Fig. 6).

## Discussion

This study used integrated in vitro and computational models to understand if, and how, tissue-level loading is related to neuronal

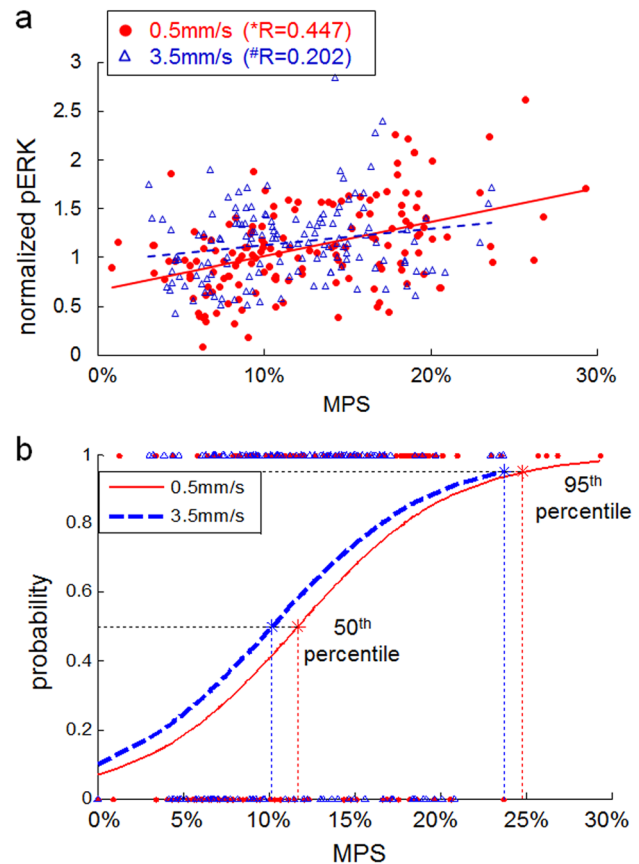


**Fig. 3** Elemental pERK expression is positively related to elemental MPS. (a) Significant positive correlations exist between normalized elemental pERK expression and elemental MPS at both 0.5 mm/s ( $R^2 = 0.200$ ,  $*p < 0.0001$ ) and 3.5 mm/s ( $R^2 = 0.041$ ,  $\#p = 0.0171$ ) distraction rates. (b) pERK expression is significantly ( $p < 0.0001$ ) regressed against elemental MPS at both distraction rates. Solid dots (●) and open triangles (Δ) represent samples in which elevated pERK expression was detected (probability of 1) or not detected (probability of 0) at each strain level for 0.5 mm/s and 3.5 mm/s, respectively. The predicted 50th-percentile thresholds for ERK phosphorylation are 11.7% for 0.5 mm/s rate, 10.2% for 3.5 mm/s; the corresponding 95th-percentile thresholds are 24.9% and 23.7% at the 0.5 mm/s and 3.5 mm/s distraction rates, respectively.

deformation and signaling via changes in the micromechanics of the collagen that surrounds afferents. Both the applied distraction magnitude and rate of loading regulated the macro- and micro-scale NCC mechanics (Table 1; Fig. 5) and the resulting neuronal responses (Figs. 2–4). In fact, neuronal expression of pERK and neuronal AR both positively correlated with the local strains in the surrounding collagen matrix at both distraction rates tested (Figs. 2–4). Interestingly, the strain thresholds for increased ERK phosphorylation and collagen fiber realignment were the same (Figs. 3 and 5), suggesting that excessive *local* fiber motion may have direct influence on neuronal responses, altering both the loading to neurons and the induction of mechanotransduction pathways, like ERK activation. As more collagen fibers reoriented toward the loading direction with increasing bulk strain, those fibers also underwent larger strains due to their elongation (Fig. 6). The increase in fiber realignment and elongation likely presents a mechanism by which the much weaker neurons reorient and deform (Fig. 4) since they are adherently embedded in the surrounding fibers matrix [38,69,70].

Under the testing conditions used in this study, both neuronal orientation and collagen fiber realignment were sensitive to the loading rate, with the greatest degree of reorientation of neurons

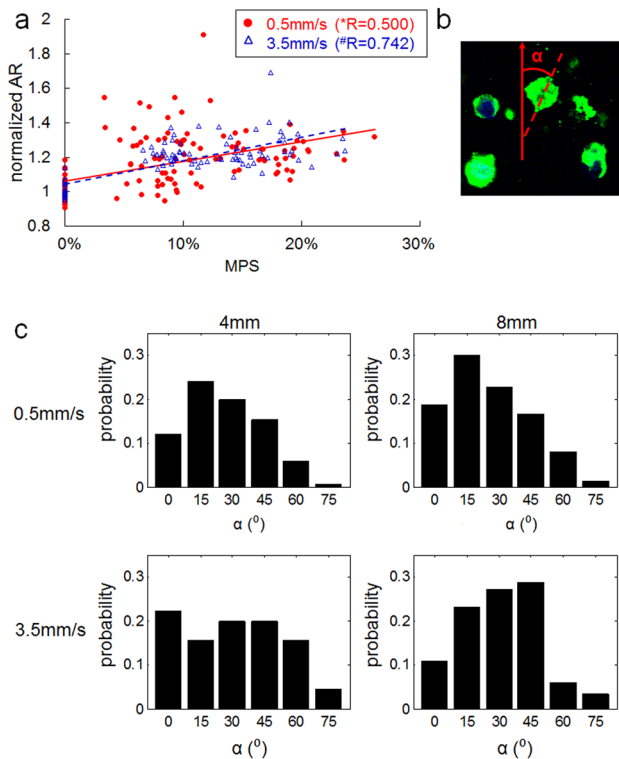


**Fig. 4** Neuronal AR and orientation toward the loading direction depend on NCC displacement and loading rate. (a) Significant correlations are detected between normalized cell AR and MPS for both 0.5 mm/s ( $*p < 0.0001$ ) and 3.5 mm/s ( $\#p < 0.0001$ ) rates of distraction. (b) Cell orientation angle ( $\alpha$ ) is measured as the angle between cell's long-axis (dotted line) and the direction of applied tension (arrow). (c) Distributions of cell orientation angles show that cell orientation angle is significantly smaller ( $p = 0.004$ ) at the slow distraction rate (0.5 mm/s) than at the fast rate (3.5 mm/s).

and collagen fibers toward the loading direction observed at the 0.5 mm/s rate (Figs. 4 and 5). This finding implies that slowly applied tissue tension enables microstructural changes of the collagen matrix that lead to more and greater changes in the micro-environment of neurons, which is not evident for similar bulk strains applied more quickly. Regardless of the macrolevel loading conditions, collagen fiber orientations within the same NCC element were spatially varied, as were the heterogeneous strains in the local collagen networks (Figs. 5 and 6). These observations, together with varied pERK production across neurons in the same NCC element (Fig. 2), suggest that even simple bulk tissue loading, like uniaxial tension, induces complicated mechanotransduction signaling in the cells embedded in fibrous tissues.

Only strains above the supraphysiologic threshold induced activation of neurons embedded in this collagenous network (Figs. 2 and 3). Behavioral hypersensitivity (i.e., pain) in the rat has been shown to be significantly correlated with the imposed FCL strain [71]; in addition, facet joint tension imposing FCL distraction in the rat points to a strain threshold of between 8% and 12% for inducing facet-mediated pain [28]. Complementary studies in the goat support excessive tensile stretch of the FCL as inducing persistent afferent activity in low-threshold ( $10.2 \pm 4.6\%$ ) and high-threshold neurons ( $47.2 \pm 9.6\%$ ) [8,10]. Our findings, that neuronal AR and ERK phosphorylations were also correlated with the applied strain and that a corresponding strain threshold (10–12%) for activation of ERK signaling in the NCCs (Figs. 2–4) was similarly evident, provide additional evidence that a relevant pain threshold for FCL loading exists between 8% and 12% depending on the rate of loading, activation metric, and/or pathologic marker of interest. Altered neuronal responses,

indicated by significant increases in ERK phosphorylation, occurred under the same loading conditions as those that induced substantial changes in collagen fiber orientation and at bulk strains greater than the physiologic limit (Figs. 2 and 5). Biomechanical studies using the same QPLI methods with isolated FCLs detect collagen fiber disorganization at strains that induce pain in vivo [16,25]. Such collagen fiber realignment may be due to the redistribution of forces among intact fibers after other load-bearing fibers fail, which has been reported at between 6% and 22% [72]. Indeed, this strain estimate of collagen fiber failure in ligaments is consistent with the fiber strains predicted by our DFN model at bulk strains simulating painful loading conditions (Fig. 6). However, this was not tested explicitly since neither of the experimental nor the computational approaches used in the current study enable measuring, or modeling, fiber failure. Nonetheless, the integrated collagen fiber kinematics and neuronal responses in the current study (Figs. 3 and 5) support the notion that microstructural collagen reorganization in the FCL can occur concurrently with altered neuronal responses at supraphysiologic strains and may be relevant to the induction of ligament pain [16,25].

The transition from isotropic to anisotropic collagen reorganization with increasing applied bulk strain (Fig. 5) is likely related to the bending–stretching transition of collagen fibers, which leads to strain hardening [49]. A characteristic strain hardening response has been documented with collagen constructs under tension and shear [73,74]. Indeed, a shift from a compliant to a stiffening regime has been reported at approximately 10% strain for gels with a collagen density of 2 mg/ml [74], which is comparable to the transition point that was evident between the two phases of fiber realignment in our study (Fig. 5). Collagen networks under shear exhibit strain hardening that starts around the transition between collagen fiber bending and stretching, with an energy cross-over slightly above 10% strain from a bending-dominated domain to a stretching-dominated domain for both single fibers and the network [49]. Stiffening of the collagen network may substantially increase the loading exerted on the embedded neurons even with small increase in the applied bulk strain, leading to persistent changes in neuronal activity after the strain hardening threshold is exceeded.

In addition to strain magnitude, the applied loading rate also regulates some, but not all, of the responses of neurons and collagen measured in this study. The greatest degrees of collagen fiber realignment and cell reorientation that occurred at the slow loading rate (Figs. 4 and 5) may be due to the viscoelastic properties of the neurons and their surrounding collagen matrix [75–77]. Viscoelasticity may limit fiber rotation and stretch during rapid NCC stretch because hydrogen bonds between and within the collagen molecules are less likely to break under rapid loading [78,79]. This resistance to fiber movement and deformation may limit fiber realignment toward the loading direction more in the NCCs loaded at 3.5 mm/s than at 0.5 mm/s (Fig. 5). Of note, continuous fiber reorientation during loading at 3.5 mm/s is not measured in this study due to limitations with the acquisition rate of the QPLI data. Since the circular variances measured at 4 mm were not different from each other at both rates nor from the unloaded control levels (Fig. 5), there is not expected to be different adaptation of collagen to tension at low magnitudes. Yet, because there was significantly less fiber realignment at 8 mm distraction at the faster rate loading (Fig. 5), the corresponding transition point for fiber realignment at 3.5 mm/s is expected to be higher than the threshold at 0.5 mm/s loading rate. Accordingly, that transition point will also be greater than the strain threshold (10.2%) measured for ERK phosphorylation at 3.5 mm/s (Fig. 3), suggesting that collagen microstructure and neuronal activation may not parallel each other in all loading conditions, particularly for higher loading rates. However, further studies are needed to fully understand those relationships.

Since the nonlinear properties of collagen and neurons can induce higher stress and less stress relaxation in tissue undergoing more rapid stretch [5,77,80], neurons stretched at the fast rate

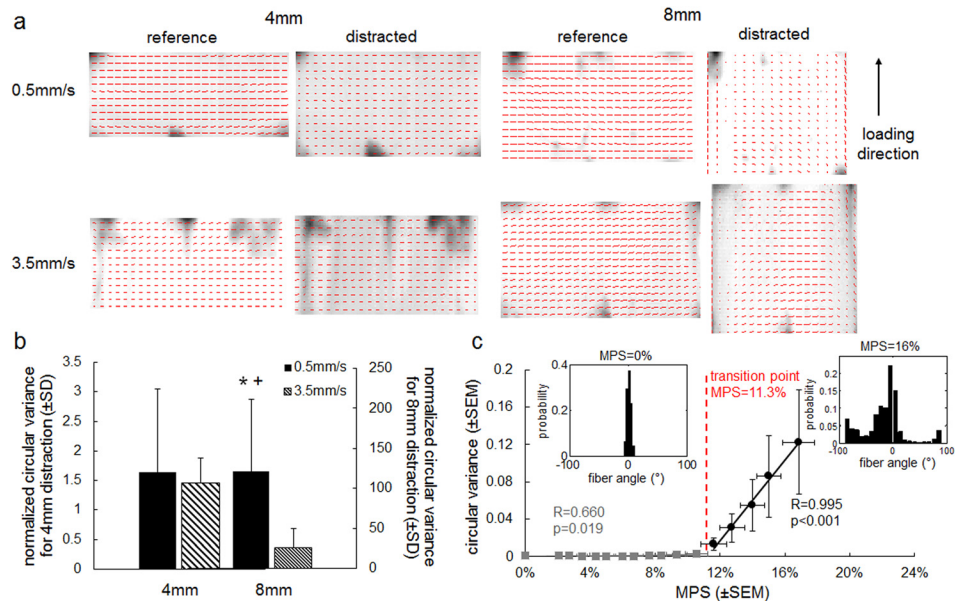


**Fig. 5** For the 0.5 mm/s loading rate, fiber realignment exhibits a switchlike response. (a) Representative collagen fiber alignment maps in two adjacent elements before (reference) and at maximal distraction (distracted) show different fiber realignment responses depending on both the distraction magnitude and rate. The direction of the orientation vector indicates the average fiber alignment direction measured through the NCC thickness and its length represents the alignment strength in that direction. Fiber reorientation toward the loading direction is apparent by the changes in the length of the orientation vectors and their directions toward the vertical direction, with the most realignment along the lateral edges (indicated by vertically orientated vectors). (b) Quantification of the normalized circular variance measures the degree of fiber realignment in the distracted configuration relative to the unloaded reference and indicates significantly more collagen fiber realignment at 8 mm of distraction at 0.5 mm/s than at either 4 mm at the same rate ( $*p = 0.009$ ) or 8 mm at the higher distraction rate ( $^+p = 0.040$ ). (c) The mean circular variance of collagen fiber orientation angles during loading at 0.5 mm/s exhibits a biphasic response with increasing applied strain (MPS), with a transition point of 11.3% strain estimated. The insets show representative distributions of collagen fiber alignment angles before (0%) and after (16%) evident fiber realignment occurs.

were hypothesized to experience greater loads and to exhibit elevated activity compared to those undergoing slower loading. However, no difference in pERK production was observed between the two rates, regardless of the distraction magnitude (Fig. 2). This may be due to the fact that there is only a sevenfold difference between the two distraction rates tested in this study, owing to limitations with the mechanical testing device in reliably imposing such relatively small displacement. Additional loading rates at several orders of magnitude higher than those tested here are needed to meaningfully evaluate the effects of neuronal signaling as a function of loading rate, particularly at rates simulating traumatic loading, which can reach as high as 500%/s [30].

Considering previous biomechanical and neurophysiological findings, our results can begin to elucidate possible mechanisms by which supraphysiologic ligament deformation modulates responses in the neurons embedded in the collagenous tissue of that ligament. When the bulk tissue strain remains within the physiologic limit (~8–12%), collagen fibers undergo almost no realignment but may bend and/or uncrimp to accommodate macroscopic deformation [72,81–83]; during that regime, the fibers experience small strains that are even lower than the bulk strain (Figs. 5 and 6). Minimal changes in the collagen fiber alignment and axial strains can lead to small-to-negligible changes in the local stresses with increasing tissue strain corresponding to the initial compliant mechanical response of the collagen network [49,74]. Neurons may still be loaded during this compliant regime due to collagen fiber motions and the Poisson effect, but at levels within their physiologic tolerance. That notion is supported by the same degree of pERK being evident in NCCs distracted to

simulate nonpainful strains as in the unloaded control samples (Figs. 2 and 3). When supraphysiologic bulk strains are reached as in the cases for painful FCL loading [28,71], substantial collagen fiber realignment toward the loading direction occurs (Figs. 5 and 6), which is likely due to the molecular bonds between collagen fibers breaking. As some fibers reorient along the loading direction and others remain unaligned, the collagen network sustains highly inhomogeneous strains, with a few load-bearing fibers sustaining axial strains that exceed the applied bulk strain. These fibers undergo excessively large local strains along the gel's loading axis to accommodate the applied macroscopic deformation, as the fibers oriented off-axis relative to the loading direction sustain strains that are less than the applied bulk strain. Further, stretching of those aligned fibers is a potential mechanism by which strain hardening rapidly increases stress in the collagen network at large bulk strains [49,74].

Excessive collagen fiber motions and stretch accommodating the large macroscopic tissue deformation may deform and reorient the soft neurons embedded in the collagen matrix (Fig. 4) to a degree exceeding the physiologic range. Fiber forces can be transmitted to compress or stretch neurons via direct contact and/or cell surface receptors with stress concentrations at the adhesion sites [25,26,84]. ERK signaling in neurons can occur within 1 min in response to cellular deformation and/or stress exceeding the mechanical tolerance of neurons [39–41,44]. Indeed, we measured pERK immediately after loading, which is at the time point when ERK phosphorylation is first induced after tissue injury [44]. Activation of ERK signaling can produce persistent changes in neurons, such as increased excitability, altered expression of ion

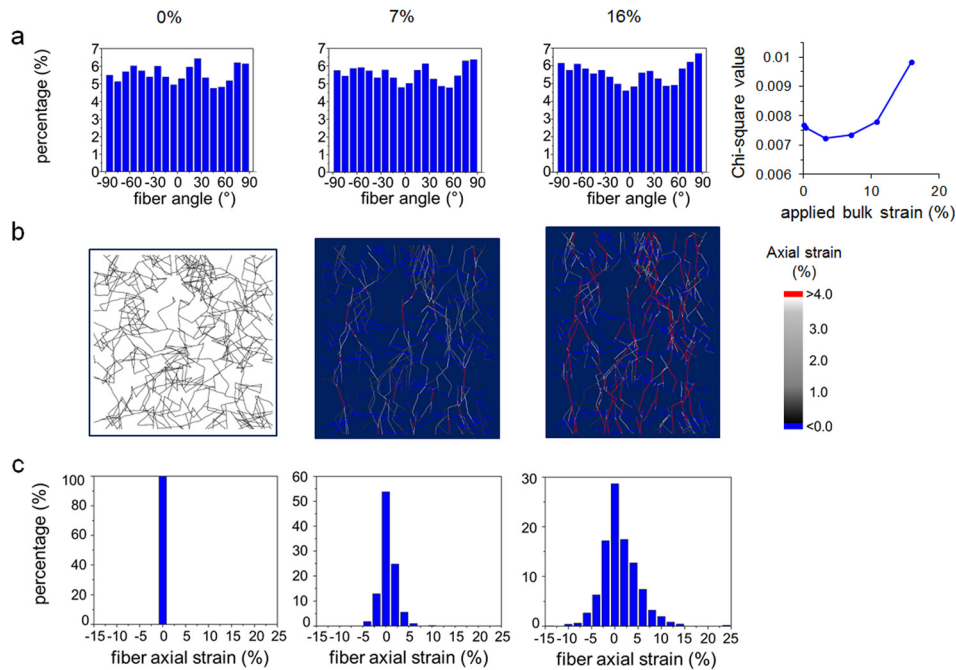


**Fig. 6 DFN modeling predicts that collagen fiber realignment and fiber strain increase with bulk strain. (a) The distribution of fiber angle indicates more realignment toward the loading direction ( $\pm 90$  deg) at 16% strain, which is different from the uniform distributions that are observed at 0% and 7% strain. Plotting the Chi-squared statistic against the applied bulk strain shows that the fiber angle distribution becomes less uniform with increasing strain above 10%. (b) Visualization of the heterogeneous fiber axial strains during network loading shows more fibers under large tensile strain as more fibers realign toward the loading direction at 16% bulk strain compared to 0% and 7% strains. (c) Distributions of fiber axial strains show that most fibers have strains lower than the applied bulk strain and both compressive and tensile fiber strains increase with increasing bulk strain.**

channels and neuromodulators, and nociceptive signaling [43–45]. Although significantly less fiber reorientation was generated by the faster rate (Fig. 5), pERK expression was not different between the two loading rates tested (Fig. 2), suggesting that mechanical factors other than collagen fiber kinematics may also contribute to neuron activation after tissue loading. Elevated stress that has been reported in ligaments due to increased loading rate [5] may induce mechanotransduction in neurons under rapidly applied macroscale tension; indeed ligament stress does correlate with neuronal responses [85]. To fully understand the mechanisms underlying neuronal activity in response to different loading conditions, it is necessary to define the relationships between macro- and microscale mechanics and neuronal loading and signaling.

Although the integrated experimental and computational models used here enable measurement of neuronal and collagen responses across length scales, there are several limitations that prevent fully defining the relationships between tissue mechanics and neuronal activation. Facet capsular and other ligaments have varied fiber organization and density in different subregions where nerves have been identified and across different anatomic ligaments [1,86–89]. The specific anatomy of a ligament can lead to varied macroscopic and microscopic mechanical responses especially for varied loading directions and under different loading rates. These complicated macroscale local environments drive different signaling responses in the neurons embedded in those regions with varied microstructures. Certainly, the effects of fiber orientation and density could be tested in this system using NCCs with prescribed collagen alignment and different concentrations to better understand if the neuronal response to tissue loading is sensitive to the initial fiber alignment and/or density. Using gels with collagen fibers pre-aligned along the loading direction or even using nonfibrous substrates, it is possible to explicitly test if the

11% strain threshold for increased ERK phosphorylation determined by the altered collagen fiber kinematics in this study is also an inherent threshold for neuronal activation.

An additional limitation of the NCC system is the use of cortical neurons, which are taken from the central nervous system, whereas the ligaments are innervated by peripheral neurons. Although both cortical neurons and primary sensory neurons have been reported to sustain similar morphological impairments and altered electrophysiological manifestations in response to stretch injury [7,10,38,90–92], they are functionally different and have different extracellular environments *in vivo*. Those local environments can alter their postinjury cellular cascades, which can induce distinct inflammatory responses and regenerative capacity after mechanical stimulation [93,94]. Future work using dorsal root ganglion neurons seeded in the NCC system would better simulate the ligament system and provide a platform for probing pain-related neuronal responses in the periphery. An additional shortcoming of this study is the measurement of total pERK expression and not the neuron-localized pERK. Total pERK was assessed in order to account for the possibility that the plasma membrane may be disrupted by the applied loading [95] and that pERK might “leak out” of neurons from their mechanical injury during distraction. Although total pERK and neuron-localized pERK in the NCC system have been shown to similarly correlate with the applied MPS [96], differentiating the effects on intracellular and extracellular pERK may provide additional insights in future studies. Further studies directly comparing pERK (and other neuronal mediators) and collagen realignment would provide important insight about these and other regulatory processes in neurons.

In addition, although fibers have been reported to uncrimp during tensile loading of ligaments in animal and computational studies [72,82], that additional mechanism of fiber deformation was

not included in the DFN model, but may affect network strain stiffening and reorganization responses under loading. The simple fibrous network model used does not include neurons; this is adequate for investigating the matrix and fiber mechanics of the NCCs due to the high compliance and low contractility of neurons. Nonetheless, the incorporation of neuronal morphology and surface receptors would better represent the in vivo conditions and enable more explicit measurements of neuronal stresses and strains under load. However, the 2D DFN model did capture the important mechanical aspects, including nonaffine stiffening and bending–stretching transition, of isotropic collagen networks and predicted a fiber realignment response mimicking the QPLI data from the 3D NCCs (Figs. 5 and 6). Nevertheless, additional parametric studies are needed to determine the minimum fiber density required in the network to ensure that quantitative results obtained from the model are statistically significant.

In summary, this study supports the hypothesis that tissue-level strains are associated with neuronal responses likely via changes in the local collagen fiber mechanics. Distraction magnitude and rate modulate macroscopic mechanics of the NCCs as well as the degree of collagen fiber realignment, which correspond to altered neuronal shape, orientation, and pERK production. ERK phosphorylation is *only* significantly increased at suprphysiologic strains, under conditions in which collagen fibers exhibit evident realignment toward the loading direction and high axial strains. Together, these data suggest an association between neuronal activation and the switchlike collagen micromechanical response. Although additional studies are needed to more fully understand the associations between the mechanical and sensory functions of ligaments, this study begins to define important potential relationships between aspects of neuronal activation and tissue mechanics across length scales. Findings also identify possible aspects of the mechanotransduction pathways leading to neuronal activation and dysfunction following excessive ligament loading.

## Acknowledgment

This work was supported by the grants from the NIH (U01EB016638 and R01EB017753) and the NSF (CMMI-1312392). The authors thank Dr. David Meaney at the University of Pennsylvania for generously providing the neurons used in this study. The authors also thank Dr. Abhilash Nair for developing the DFN model that was adapted in the current study.

## References

- [1] Kallakuri, S., Li, Y., Chen, C., and Cavanaugh, J. M., 2012, "Innervation of Cervical Ventral Facet Joint Capsule: Histological Evidence," *World J. Orthop.*, **3**(2), pp. 10–14.
- [2] Yahia, L. H., and Newman, N., 1991, "Innervation of Spinal Ligaments of Patients With Disc Herniation. An Immunohistochemical Study," *Pathol. Res. Pract.*, **187**(8), pp. 936–938.
- [3] Petrie, S., Collins, J. G., Solomonow, M., Wink, C., Chuinard, R., and D'Ambrosia, R., 1998, "Mechanoreceptors in the Human Elbow Ligaments," *J. Hand Surg. Am.*, **23**(3), pp. 512–518.
- [4] Schultz, R. A., Miller, D. C., Kerr, C. S., and Micheli, L., 1984, "Mechanoreceptors in Human Cruciate Ligaments. A Histological Study," *J. Bone Joint Surg. Am.*, **66**(7), pp. 1072–1076.
- [5] Solomonow, M., 2004, "Ligaments: A Source of Work-Related Musculoskeletal Disorders," *J. Electromyogr. Kinesiol.*, **14**(1), pp. 49–60.
- [6] Winkelstein, B. A., 2011, "How Can Animal Models Inform on the Transition to Chronic Symptoms in Whiplash?" *Spine*, **36**(Suppl. 25), pp. S218–225.
- [7] Kallakuri, S., Singh, A., Lu, Y., Chen, C., Patwardhan, A., and Cavanaugh, J. M., 2008, "Tensile Stretching of Cervical Facet Joint Capsule and Related Axonal Changes," *Eur. Spine J.*, **17**(4), pp. 556–563.
- [8] Chen, C., Lu, Y., Kallakuri, S., Patwardhan, A., and Cavanaugh, J. M., 2006, "Distribution of A-Delta and C-Fiber Receptors in the Cervical Facet Joint Capsule and Their Response to Stretch," *J. Bone Joint Surg. Am.*, **88**(8), pp. 1807–1816.
- [9] Kras, J. V., Tanaka, K., Gilliland, T. M., and Winkelstein, B. A., 2013, "An Anatomical and Immunohistochemical Characterization of Afferents Innervating the C6-C7 Facet Joint After Painful Joint Loading in the Rat," *Spine*, **38**(6), pp. E325–331.
- [10] Lu, Y., Chen, C., Kallakuri, S., Patwardhan, A., and Cavanaugh, J. M., 2005, "Neural Response of Cervical Facet Joint Capsule to Stretch: A Study of Whiplash Pain Mechanism," *Stapp Car Crash J.*, **49**, pp. 49–65.
- [11] Crosby, N. D., Gilliland, T. M., and Winkelstein, B. A., 2014, "Early Afferent Activity From the Facet Joint After Painful Trauma to Its Capsule Potentiates Neuronal Excitability and Glutamate Signaling in the Spinal Cord," *Pain*, **155**(9), pp. 1878–1887.
- [12] Lee, K. E., and Winkelstein, B. A., 2009, "Joint Distraction Magnitude is Associated With Different Behavioral Outcomes and Substance P Levels for Cervical Facet Joint Loading in the Rat," *J. Pain*, **10**(4), pp. 436–445.
- [13] Lee, K. E., Davis, M. B., and Winkelstein, B. A., 2008, "Capsular Ligament Involvement in the Development of Mechanical Hyperalgesia After Facet Joint Loading: Behavioral and Inflammatory Outcomes in a Rodent Model of Pain," *J. Neurotrauma*, **25**(11), pp. 1383–1393.
- [14] Quinn, K. P., Dong, L., Golder, F. J., and Winkelstein, B. A., 2010, "Neuronal Hyperexcitability in the Dorsal Horn After Painful Facet Joint Injury," *Pain*, **151**(2), pp. 414–421.
- [15] Quinn, K. P., Lee, K. E., Ahaghotu, C. C., and Winkelstein, B. A., 2007, "Structural Changes in the Cervical Facet Capsular Ligament: Potential Contributions to Pain Following Subfailure Loading," *Stapp Car Crash J.*, **51**, pp. 169–187.
- [16] Quinn, K. P., Bauman, J. A., Crosby, N. D., and Winkelstein, B. A., 2010, "Anomalous Fiber Realignment During Tensile Loading of the Rat Facet Capsular Ligament Identifies Mechanically Induced Damage and Physiological Dysfunction," *J. Biomech.*, **43**(10), pp. 1870–1875.
- [17] Crosby, N. D., Weisshaar, C. L., and Winkelstein, B. A., 2013, "Spinal Neuronal Plasticity is Evident Within 1 Day After a Painful Cervical Facet Joint Injury," *Neurosci. Lett.*, **542**, pp. 102–106.
- [18] Kras, J. V., Kartha, S., and Winkelstein, B. A., 2015, "Intra-Articular Nerve Growth Factor Regulates Development, But Not Maintenance, of Injury-Induced Facet Joint Pain & Spinal Neuronal Hypersensitivity," *Osteoarthritis and Cartilage*, **23**(11) pp. 1999–2008.
- [19] Rosso, F., Giordano, A., Barbarisi, M., and Barbarisi, A., 2004, "From Cell-ECM Interactions to Tissue Engineering," *J. Cell. Physiol.*, **199**(2), pp. 174–180.
- [20] Barros, C. S., Franco, S. J., and Müller, U., 2011, "Extracellular Matrix: Functions in the Nervous System," *Cold Spring Harbor Perspect. Biol.*, **3**(1), p. a005108.
- [21] Spedden, E., White, J. D., Naumova, E. N., Kaplan, D. L., and Staii, C., 2012, "Elasticity Maps of Living Neurons Measured by Combined Fluorescence and Atomic Force Microscopy," *Biophys. J.*, **103**(5), pp. 868–877.
- [22] Wenger, M. P. E., Bozec, L., Horton, M. A., and Mesquida, P., 2007, "Mechanical Properties of Collagen Fibrils," *Biophys. J.*, **93**(4), pp. 1255–1263.
- [23] Lopez-Garcia, M. D. C., Beebe, D. J., and Crone, W. C., 2010, "Young's Modulus of Collagen at Slow Displacement Rates," *Biomed. Mater. Eng.*, **20**(6), pp. 361–369.
- [24] Tower, T. T., Neidert, M. R., and Tranquillo, R. T., 2002, "Fiber Alignment Imaging During Mechanical Testing of Soft Tissues," *Ann. Biomed. Eng.*, **30**(10), pp. 1221–1233.
- [25] Quinn, K. P., and Winkelstein, B. A., 2009, "Vector Correlation Technique for Pixel-Wise Detection of Collagen Fiber Realignment during Injurious Tensile Loading," *J. Biomed. Opt.*, **14**(5), p. 054010.
- [26] Sander, E. A., Stylianopoulos, T., Tranquillo, R. T., and Barocas, V. H., 2009, "Image-Based Multiscale Modeling Predicts Tissue-Level and Network-Level Fiber Reorganization in Stretched Cell-Compacted Collagen Gels," *Proc. Natl. Acad. Sci. U.S.A.*, **106**(42), pp. 17675–17680.
- [27] Quinn, K. P., and Winkelstein, B. A., 2008, "Altered Collagen Fiber Kinematics Define the Onset of Localized Ligament Damage During Loading," *J. Appl. Physiol.*, **105**(6), pp. 1881–1888.
- [28] Dong, L., Quindlen, J. C., Lipschutz, D. E., and Winkelstein, B. A., 2012, "Whiplash-Like Facet Joint Loading Initiates Glutamatergic Responses in the DRG and Spinal Cord Associated With Behavioral Hypersensitivity," *Brain Res.*, **1461**, pp. 51–63.
- [29] Schenck, R. C., Kovach, I. S., Agarwal, A., Brummett, R., Ward, R. A., Lantot, D., and Athanasiou, K. A., 1999, "Cruciate Injury Patterns in Knee Hyperextension: A Cadaveric Model," *Arthroscopy*, **15**(5), pp. 489–495.
- [30] Panjabi, M. M., Cholewicki, J., Nibu, K., Grauer, J., and Vahldiek, M., 1998, "Capsular Ligament Stretches During In Vitro Whiplash Simulations," *J. Spinal Disord.*, **11**(3), pp. 227–232.
- [31] Noyes, F. R., DeLucas, J. L., and Torvik, P. J., 1974, "Biomechanics of Anterior Cruciate Ligament Failure: An Analysis of Strain-Rate Sensitivity and Mechanisms of Failure in Primates," *J. Bone Jt. Surg. Am.*, **56**(2), pp. 236–253.
- [32] Vader, D., Kabla, A., Weitz, D., and Mahadevan, L., 2009, "Strain-Induced Alignment in Collagen Gels," *PLoS One*, **4**(6), p. e5902.
- [33] Cullen, D. K., Simon, C. M., and LaPlaca, M. C., 2007, "Strain Rate-Dependent Induction of Reactive Astroglial Cell Death in Three-Dimensional Neuronal-Astrocytic Co-Cultures," *Brain Res.*, **1158**, pp. 103–115.
- [34] Geddes, D. M., Cargill, R. S., and LaPlaca, M. C., 2003, "Mechanical Stretch to Neurons Results in a Strain Rate and Magnitude-Dependent Increase in Plasma Membrane Permeability," *J. Neurotrauma*, **20**(10), pp. 1039–1049.
- [35] Delmas, P., Hao, J., and Rodat-Despoix, L., 2011, "Molecular Mechanisms of Mechanotransduction in Mammalian Sensory Neurons," *Nat. Rev. Neurosci.*, **12**(3), pp. 139–153.
- [36] Martinac, B., 2004, "Mechanosensitive Ion Channels: Molecules of Mechanotransduction," *J. Cell Sci.*, **117**(Pt 12), pp. 2449–2460.
- [37] Raoux, M., Rodat-Despoix, L., Azorin, N., Giamarchi, A., Hao, J., Maingret, F., Crest, M., Coste, B., and Delmas, P., 2007, "Mechanosensor Channels in Mammalian Somatosensory Neurons," *Sensors (Basel)*, **7**(9), pp. 1667–1682.

- [38] Hemphill, M. A., Dabiri, B. E., Gabriele, S., Kerscher, L., Franck, C., Goss, J. A., Alford, P. W., and Parker, K. K., 2011, "A Possible Role for Integrin Signaling in Diffuse Axonal Injury," *PLoS One*, **6**(7), p. e22899.
- [39] Chaturvedi, L. S., Gayer, C. P., Marsh, H. M., and Basson, M. D., 2008, "Repetitive Deformation Activates Src-Independent FAK-Dependent ERK Mitogenic Signals in Human Caco-2 Intestinal Epithelial Cells," *Am. J. Physiol. Cell Physiol.*, **294**(6), pp. C1350–1361.
- [40] Samarakoon, R., and Higgins, P. J., 2003, "Pp60c-Src Mediates ERK Activation/Nuclear Localization and PAI-1 Gene Expression in Response to Cellular Deformation," *J. Cell. Physiol.*, **195**(3), pp. 411–420.
- [41] Neary, J. T., Kang, Y., Willoughby, K. A., and Ellis, E. F., 2003, "Activation of Extracellular Signal-Regulated Kinase by Stretch-Induced Injury in Astrocytes Involves Extracellular ATP and P2 Purinergic Receptors," *J. Neurosci.*, **23**(6), pp. 2348–2356.
- [42] Stamboulian, S., Choi, J.-S., Ahn, H.-S., Chang, Y.-W., Tyrrell, L., Black, J. A., Waxman, S. G., and Dib-Hajj, S. D., 2010, "ERK1/2 Mitogen-Activated Protein Kinase Phosphorylates Sodium Channel Na(V)1.7 and Alters Its Gating Properties," *J. Neurosci.*, **30**(5), pp. 1637–1647.
- [43] Cheng, J.-K., and Ji, R.-R., 2008, "Intracellular Signaling in Primary Sensory Neurons and Persistent Pain," *Neurochem. Res.*, **33**(10), pp. 1970–1978.
- [44] Gao, Y.-J., and Ji, R.-R., 2009, "c-Fos and pERK, Which is a Better Marker for Neuronal Activation and Central Sensitization After Noxious Stimulation and Tissue Injury?" *Open Pain J.*, **2**(1), pp. 11–17.
- [45] Ji, R. R., Baba, H., Brenner, G. J., and Woolf, C. J., 1999, "Nociceptive-Specific Activation of ERK in Spinal Neurons Contributes to Pain Hypersensitivity," *Nat. Neurosci.*, **2**(12), pp. 1114–1119.
- [46] Kras, J. V., Weisshaar, C. L., Quindlen, J., and Winkelstein, B. A., 2013, "Brain-Derived Neurotrophic Factor is Upregulated in the Cervical Dorsal Root Ganglia and Spinal Cord and Contributes to the Maintenance of Pain From Facet Joint Injury in the Rat," *J. Neurosci. Res.*, **91**(10), pp. 1312–1321.
- [47] Sander, E. A., Tranquillo, R. T., and Barocas, V. H., 2009, "Image-Based Multiscale Structural Models of Fibrous Engineered Tissues," Annual International Conference of the IEEE Engineering in Medicine and Biology Society (EMBC 2009), Minneapolis, MN, Sept. 3–6, pp. 4270–4272.
- [48] Lake, S. P., and Barocas, V. H., 2011, "Mechanical and Structural Contribution of Non-Fibrillar Matrix in Uniaxial Tension: A Collagen-Agarose Co-Gel Model," *Ann. Biomed. Eng.*, **39**(7), pp. 1891–1903.
- [49] Nair, A., Baker, B. M., Trappmann, B., Chen, C. S., and Shenoy, V. B., 2014, "Remodeling of Fibrous Extracellular Matrices by Contractile Cells: Predictions From Discrete Fiber Network Simulations," *Biophys. J.*, **107**(8), pp. 1829–1840.
- [50] Aghvami, M., Barocas, V. H., and Sander, E. A., 2013, "Multiscale Mechanical Simulations of Cell Compacted Collagen Gels," *ASME J. Biomech. Eng.*, **135**(7), p. 071004.
- [51] Hadi, M. F., Sander, E. A., Ruberti, J. W., and Barocas, V. H., 2012, "Simulated Remodeling of Loaded Collagen Networks Via Strain-Dependent Enzymatic Degradation and Constant-Rate Fiber Growth," *Mech. Mater.*, **44**, pp. 72–82.
- [52] Evans, M. C., and Barocas, V. H., 2009, "The Modulus of Fibroblast-Populated Collagen Gels is Not Determined by Final Collagen and Cell Concentration: Experiments and an Inclusion-Based Model," *ASME J. Biomech. Eng.*, **131**(10), p. 101014.
- [53] Dong, L., Guarino, B. B., Jordan-Sciutto, K. L., and Winkelstein, B. A., 2011, "Activating Transcription Factor 4, A Mediator of the Integrated Stress Response, is Increased in the Dorsal Root Ganglia Following Painful Facet Joint Distraction," *Neuroscience*, **193**, pp. 377–386.
- [54] Bonner, T. J., Newell, N., Karunaratne, A., Pullen, A. D., Amis, A. A. M. J., Bull, A., and Masouros, S. D., 2015, "Strain-Rate Sensitivity of the Lateral Collateral Ligament of the Knee," *J. Mech. Behav. Biomed. Mater.*, **41**, pp. 261–270.
- [55] Crisco, J. J., Moore, D. C., and McGovern, R. D., 2002, "Strain-Rate Sensitivity of the Rabbit MCL Diminishes at Traumatic Loading Rates," *J. Biomech.*, **35**(10), pp. 1379–1385.
- [56] Patel, T. P., Man, K., Firestone, B. L., and Meaney, D. F., 2015, "Automated Quantification of Neuronal Networks and Single-Cell Calcium Dynamics Using Calcium Imaging," *J. Neurosci. Methods*, **243**, pp. 26–38.
- [57] MacArthur, M. W., and Thornton, J. M., 1993, "Conformational Analysis of Protein Structures Derived From NMR Data," *Proteins*, **17**(3), pp. 232–251.
- [58] Miller, K. S., Connizzo, B. K., and Soslowky, L. J., 2012, "Collagen Fiber Re-Alignment in a Neonatal Developmental Mouse Supraspinatus Tendon Model," *Ann. Biomed. Eng.*, **40**(5), pp. 1102–1110.
- [59] Weisshaar, C. L., Dong, L., Bowman, A. S., Perez, F. M., Guarino, B. B., Sweitzer, S. M., and Winkelstein, B. A., 2010, "Metabotropic Glutamate Receptor-5 and Protein Kinase C-Epsilon Increase in Dorsal Root Ganglion Neurons and Spinal Glial Activation in an Adolescent Rat Model of Painful Neck Injury," *J. Neurotrauma*, **27**(12), pp. 2261–2271.
- [60] Lee, K. E., Franklin, A. N., Davis, M. B., and Winkelstein, B. A., 2006, "Tensile Cervical Facet Capsule Ligament Mechanics: Failure and Subfailure Responses in the Rat," *J. Biomech.*, **39**(7), pp. 1256–1264.
- [61] Kras, J. V., Dong, L., and Winkelstein, B. A., 2014, "Increased Interleukin-1 $\alpha$  and Prostaglandin E2 Expression in the Spinal Cord at 1 Day After Painful Facet Joint Injury: Evidence of Early Spinal Inflammation," *Spine*, **39**(3), pp. 207–212.
- [62] Zhang, S., Nicholson, K. J., Smith, J. R., Gilliland, T. M., Syré, P. P., and Winkelstein, B. A., 2013, "The Roles of Mechanical Compression and Chemical Irritation in Regulating Spinal Neuronal Signaling in Painful Cervical Nerve Root Injury," *Stapp Car Crash J.*, **57**, pp. 219–242.
- [63] Atanasov, D., 2010, "Two-Phase Linear Regression Model," MATLAB Central File Exchange, The Mathworks, Natick, MA, <http://www.mathworks.com/matlabcentral/fileexchange/26804-two-phase-linear-regression-model>
- [64] Diniz, C. A. R., and Brochi, L. C., 2005, "Robustness of Two-Phase Regression Tests," *Revstat—Stat. J.*, **3**(1), pp. 1–18.
- [65] Koul, H. L., Qian, L., and Sargailis, D., 2003, "Asymptotics of M-Estimators in Two-Phase Linear Regression Models," *Stochastic Processes Appl.*, **103**(1), pp. 123–154.
- [66] Bain, A. C., Raghupathi, R., and Meaney, D. F., 2001, "Dynamic Stretch Correlates to Both Morphological Abnormalities and Electrophysiological Impairment in a Model of Traumatic Axonal Injury," *J. Neurotrauma*, **18**(5), pp. 499–511.
- [67] Hubbard, R. D., and Winkelstein, B. A., 2008, "Dorsal Root Compression Produces Myelinated Axonal Degeneration Near the Biomechanical Thresholds for Mechanical Behavioral Hypersensitivity," *Exp. Neurol.*, **212**(2), pp. 482–489.
- [68] McDonald, J. H., 2014, *Handbook of Biological Statistics*, 3rd ed., Sparkly House Publishing, Baltimore, MD.
- [69] Schwartz, M. A., 2010, "Integrins and Extracellular Matrix in Mechanotransduction," *Cold Spring Harbor Perspect. Biol.*, **2**(12), p. a005066.
- [70] Spedden, E., and Staii, C., 2013, "Neuron Biomechanics Probed by Atomic Force Microscopy," *Int. J. Mol. Sci.*, **14**(8), pp. 16124–16140.
- [71] Dong, L., and Winkelstein, B. A., 2010, "Simulated Whiplash Modulates Expression of the Glutamatergic System in the Spinal Cord Suggesting Spinal Plasticity is Associated With Painful Dynamic Cervical Facet Loading," *J. Neurotrauma*, **27**(1), pp. 163–174.
- [72] Liao, H., and Belkoff, S. M., 1999, "A Failure Model for Ligaments," *J. Biomech.*, **32**(2), pp. 183–188.
- [73] Münster, S., Jawerth, L. M., Leslie, B. A., Weitz, J. I., Fabry, B., and Weitz, D. A., 2013, "Strain History Dependence of the Nonlinear Stress Response of Fibrin and Collagen Networks," *Proc. Natl. Acad. Sci. U.S.A.*, **110**(30), pp. 12197–12202.
- [74] Roeder, B. A., Kokini, K., Sturgis, J. E., Robinson, J. P., and Voytik-Harbin, S. L., 2002, "Tensile Mechanical Properties of Three-Dimensional Type I Collagen Extracellular Matrices With Varied Microstructure," *ASME J. Biomech. Eng.*, **124**(2), pp. 214–222.
- [75] Lu, Y.-B., Franze, K., Seifert, G., Steinhäuser, C., Kirchhoff, F., Wolburg, H., Guck, J., Janmey, P., Wei, E.-Q., Käs, J., and Reichenbach, A., 2006, "Viscoelastic Properties of Individual Glial Cells and Neurons in the CNS," *Proc. Natl. Acad. Sci. U.S.A.*, **103**(47), pp. 17759–17764.
- [76] Topp, K. S., and Boyd, B. S., 2006, "Structure and Biomechanics of Peripheral Nerves: Nerve Responses to Physical Stresses and Implications for Physical Therapist Practice," *Phys. Ther.*, **86**(1), pp. 92–109.
- [77] Xu, B., Li, H., and Zhang, Y., 2013, "Understanding the Viscoelastic Behavior of Collagen Matrices Through Relaxation Time Distribution Spectrum," *Biomater.*, **3**(3), p. e24651.
- [78] Silver, F. H., Seehra, G. P., Freeman, J. W., and DeVore, D., 2002, "Viscoelastic Properties of Young and Old Human Dermis: A Proposed Molecular Mechanism for Elastic Energy Storage in Collagen and Elastin," *J. Appl. Polym. Sci.*, **86**(8), pp. 1978–1985.
- [79] In't Veld, P. J., and Stevens, M. J., 2008, "Simulation of the Mechanical Strength of a Single Collagen Molecule," *Biophys. J.*, **95**(1), pp. 33–39.
- [80] Laplaca, M. C., and Prado, G. R., 2010, "Neural Mechanobiology and Neuronal Vulnerability to Traumatic Loading," *J. Biomech.*, **43**(1), pp. 71–78.
- [81] Miller, K. S., Connizzo, B. K., Feeney, E., Tucker, J. J., and Soslowky, L. J., 2012, "Examining Differences in Local Collagen Fiber Crimp Frequency Throughout Mechanical Testing in a Developmental Mouse Supraspinatus Tendon Model," *ASME J. Biomech. Eng.*, **134**(4), p. 041004.
- [82] Franchi, M., Quaranta, M., Macciocca, M., Leonardi, L., Ottani, V., Bianchini, P., Diaspro, A., and Ruggeri, A., 2010, "Collagen Fibre Arrangement and Functional Crimping Pattern of the Medial Collateral Ligament in the Rat Knee," *Knee Surg. Sports Traumatol. Arthrosc.*, **18**(12), pp. 1671–1678.
- [83] Sacks, M. S., 2003, "Incorporation of Experimentally-Derived Fiber Orientation Into a Structural Constitutive Model for Planar Collagenous Tissues," *ASME J. Biomech. Eng.*, **125**(2), pp. 280–287.
- [84] Cullen, D. K., Lessing, M. C., and LaPlaca, M. C., 2007, "Collagen-Dependent Neurite Outgrowth and Response to Dynamic Deformation in Three-Dimensional Neuronal Cultures," *Ann. Biomed. Eng.*, **35**(5), pp. 835–846.
- [85] Khalsa, P. S., Hoffman, A. H., and Grigg, P., 1996, "Mechanical States Encoded by Stretch-Sensitive Neurons in Feline Joint Capsule," *J. Neurophysiol.*, **76**(1), pp. 175–187.
- [86] Yamashita, T., Minaki, Y., Ozaktay, A. C., Cavanaugh, J. M., and King, A. I., 1996, "A Morphological Study of the Fibrous Capsule of the Human Lumbar Facet Joint," *Spine*, **21**(5), pp. 538–543.
- [87] Mommersteeg, T. J., Blankevoort, L., Kooloos, J. G., Hendriks, J. C., Kauer, J. M., and Huijskes, R., 1994, "Nonuniform Distribution of Collagen Density in Human Knee Ligaments," *J. Orthop. Res.*, **12**(2), pp. 238–245.
- [88] McLain, R. F., and Pickar, J. G., 1998, "Mechanoreceptor Endings in Human Thoracic and Lumbar Facet Joints," *Spine*, **23**(2), pp. 168–173.
- [89] Cavanaugh, J. M., Lu, Y., Chen, C., and Kallakuri, S., 2006, "Pain Generation in Lumbar and Cervical Facet Joints," *J. Bone Jt. Surg. Am.*, **88**(Suppl. 2), pp. 63–67.
- [90] Tang-Schomer, M. D., Patel, A. R., Baas, P. W., and Smith, D. H., 2010, "Mechanical Breaking of Microtubules in Axons During Dynamic Stretch

- Injury Underlies Delayed Elasticity, Microtubule Disassembly, and Axon Degeneration," *FASEB J.*, **24**(5), pp. 1401–1410.
- [91] Jaumard, N. V., Welch, W. C., and Winkelstein, B. A., 2011, "Spinal Facet Joint Biomechanics and Mechanotransduction in Normal, Injury and Degenerative Conditions," *ASME J. Biomech. Eng.*, **133**(7), p. 071010.
- [92] Magou, G. C., Pfister, B. J., and Berlin, J. R., 2015, "Effect of Acute Stretch Injury on Action Potential and Network Activity of Rat Neocortical Neurons in Culture," *Brain Res.*, **1624**, pp. 525–535.
- [93] Siddique, R., and Thakor, N., 2014, "Investigation of Nerve Injury Through Microfluidic Devices," *J. R. Soc. Interface*, **11**(90), p. 20130676.
- [94] Mietto, B. S., Mostacada, K., and Martinez, A. M. B., 2015, "Neurotrauma and Inflammation: CNS and PNS Responses," *Mediators Inflammation*, **2015**, p. 251204.
- [95] Cullen, D. K., Vernekar, V. N., and LaPlaca, M. C., 2011, "Trauma-Induced Plasmalemma Disruptions in Three-Dimensional Neural Cultures are Dependent on Strain Modality and Rate," *J. Neurotrauma*, **28**(11), pp. 2219–2233.
- [96] Zhang, S., Barocas, V. H., and Winkelstein, B. A., 2014, "Local Neuronal Loading Modulates Perikary Release in a Neuron-Collagen Gel Construct Simulating Facet Capsule Injury," 7th World Congress of Biomechanics, Boston, MA, July 6–11.